

RESEARCH

Open Access



# Assessing the Seismic Performance of Exterior Precast Concrete Joints with Ultra-High-Performance Fiber-Reinforced Concrete

Seungki Kim<sup>1</sup>, Jinwon Shin<sup>2\*</sup> and Woosuk Kim<sup>3\*</sup>

## Abstract

This study was conducted to evaluate the seismic performance of an exterior precast concrete (PC) beam–column joint with ultra-high-performance fiber-reinforced concrete (UHPFRC). Currently, 45 MPa non-shrinkage mortar is used as grouting for the connection between PC beams and columns. In this study, PC joint specimens were designed using 45 MPa non-shrinkage mortar and 120 MPa UHPFRC as a grouting agent for connecting PC members. The shear reinforcement effect of UHPFRC was confirmed to reduce shear cracks in the joint core; this trend was similar in the specimens with reduced shear rebars. The maximum moment of the test specimen with the corbel was slightly increased, but there was no significant difference, and the failure pattern also showed similar results to the specimen without the corbel. In the test specimen to which the U-shaped beam was applied, the attachment surface of ultra-high-performance concrete and normal concrete were separated, and a large decrease in strength was observed. Considering workability, U-shaped beam do not seem to have any major merits in general, such as increased strength and difficulty in manufacturing, and it was judged that it was effective to separate the PC beams from the column face through corbels. Shear reinforcement through UHPFRC is effective in relieving congestion by reducing shear reinforcement bars at the joint, and it is judged that it can be used as PC joint grouting due to its excellent fluidity.

**Keywords** Seismic performance, Precast concrete joints, Fiber, Ultra-high-performance fiber-reinforced concrete

Journal information: ISSN 1976-0485 / eISSN 2234-1315.

\*Correspondence:

Jinwon Shin  
jshin@cku.ac.kr  
Woosuk Kim  
kimw@kumoh.ac.kr

<sup>1</sup> Department of Architectural Engineering, Kumoh National Institute of Technology, 61 Daehak-ro, Gumi, Gyeongsangbuk-do, 39177, Republic of Korea

<sup>2</sup> Department of Architectural Engineering, Catholic Kwandong University Gangneung, Beomil-ro 579beon-gil, Gangneung-si, Gangwon-do 25601, Republic of Korea

<sup>3</sup> Department of Architectural Engineering, Kumoh National Institute of Technology, 61 Daehak-ro, Gumi, Gyeongsangbuk-do 39177, Republic of Korea

## 1 Introduction

Carbon reduction is a major concern for industries worldwide. The Intergovernmental Panel on Climate Change (IPCC) suggested that carbon dioxide (CO<sub>2</sub>) emissions should be reduced by about 25% compared to 2010 by 2030, and carbon neutrality should be achieved around 2070 (IPCC, 2007). As a result, in the construction industry, which emits around 25% of greenhouse gases globally and 47% of CO<sub>2</sub> (of which concrete accounts for approximately 8%), various studies on eco-friendly materials and construction methods are being actively conducted to reduce carbon emissions (Husam et al., 2019). Precast concrete (PC) systems are an eco-friendly construction technique attracting attention within this context. The PC system can reduce cement

usage and minimize waste generation through an efficient compaction process while being produced in a factory instead of on-site and can contribute to carbon reduction in the construction sector by making it easy to manufacture members using high-quality, low-carbon concrete mixtures (Na et al., 2021).

The carbon emissions of buildings compared with the PC method and the cast-in-place approach via life cycle assessment (LCA), and when producing 1 m<sup>3</sup> of concrete, PC was able to reduce carbon emissions by 10% compared to cast-in situ concrete (Dong et al., 2015). When PC members were produced on-site, there was an average CO<sub>2</sub> emissions reduction effect of 25.64% compared to factory production (Na et al., 2021). In general, PC members produced in factories emit CO<sub>2</sub> in the process of transporting them to the site after production. However, even considering this, it is possible to reduce carbon emissions, and PC systems help to reduce CO<sub>2</sub> at construction sites. PC systems have proven their carbon reduction performance through several studies.

The PC system has advantages such as reducing carbon dioxide, securing high quality and high performance, and reducing production costs, but structurally, it is difficult to integrate the PC member, and it is vulnerable to earthquakes due to low stiffness and energy absorbing ability, which causes problems due to stress discontinuity. Therefore, the earthquake resistance of PC systems is lower than that of reinforced concrete (RC) systems. If the seismic reinforcement details of the RC joint are applied to secure the seismic performance of the PC joint, the fieldwork increases because it is difficult to place the reinforcement and concrete. Several studies have been performed on joint systems using steel frames to reduce on-site work and enhance constructability.

Chang et al., (2021) developed a member-panel zone unified PC joint and they investigated the seismic performance of an internal beam–column joint. The integrated beam-joint specimen had a shear failure pattern similar to that of the cast-in situ specimen compared to the integrated column-joint specimen. Choi et al., (2013) assessed the seismic performance of a specimen fabricated by bolting a steel plate exposed at the end of the beam (where it meets the column) and the square tube of the joint, pouring the engineered cementitious composite (ECC). All specimens exhibited typical flexural failure behavior. No stress discontinuity was observed between the steel connecting member and the ECC. Ghayeb et al., (2020) fabricated a hybrid PC beam–column junction specimen by combining a steel coupler, steel tube, gusset plate, and high-strength concrete and evaluated its seismic performance. The first crack load increased by up to 70%; the plastic hinge was located outside the joint area, and displacement, load, moment, and drift

ratio all improved compared to the RC connection. Lin et al., (2021) presented a PC beam–column joint using 120 MPa UHPC core shells and assessed its seismic performance. The use of UHPC core shell effectively delayed diagonal cracks in the joints and limited the crack width to less than 0.05 mm in joint core. PC specimen exhibited the same bending failure pattern as the monolithic specimen, the equivalent damping coefficient was larger, and high energy-dissipation efficiency was demonstrated.

In the studies connecting PC joints using joint cores made of steel and concrete, etc., stress discontinuity between members was reduced, behavior similar to that of cast-in-place concrete joints was observed, and energy dissipation efficiency increased.

Parastesh et al., (2014) presented a new ductile moment-resisting beam–column connection to provide structural integrity and minimize on-site work and cast-in situ concrete. The crack reduction and ductility of the joint were improved with diagonal rebars and closed stirrups, and the energy-dissipation capacity was improved. Wahjudi et al., (2014) evaluated seismic performance applying the connection reinforcement bars of the beam and joint in the form of an L-and-U bent. All the PC specimens exhibited lower strengths than the monolithic specimens, but the ductility values were slightly higher. Deng et al., (2020) conducted an experiment by fabricating a beam–column joint using 90 MPa high ductile concrete (HDC) that was fiber-reinforced to boost the seismic performance and solve the congestion of reinforcement bars and construction complexity. The connection was reinforced through the conversion to beam end failure. Maya et al., (2013) proposed and evaluated a beam–column connection method using ultra-high-performance fiber-reinforced concrete (UHPFRC) to achieve a short reinforcement bar splice length. Although more than 95% of the nominal strength was achieved at 10 d<sub>b</sub>, brittle failure occurred at the nominal capacity load level.

Research has been conducted on improving the ductility ability by changing the amount of reinforcement bar and the placing method of reinforcement bar and enhancing joint performance by bolstering the strength of grouting concrete. Previous studies have confirmed that shear force and damage resistance are enhanced when high-performance concrete is used for joint grouting. It is judged that it is possible to reduce the shear rebar of the joint by using high-performance concrete (HPC), but the effect of fiber incorporation is evaluated only on crack and damage resistance, so it is necessary to evaluate the ductility ability of the joint according to the concrete characteristics. In addition, as the application of UHPFRC increased, it was judged that a study on the mixture with improved properties for joint application was necessary.

In this study, seismic performance and shear reinforcement effects were investigated by fabricating an exterior PC beam–column joint using UHPFRC. A total of seven specimens were produced, and two types of grouting non-shrinkage mortar and UHPFRC were employed to analyze the effect of grouting performance. The number of stirrups in the beam end and joint core was reduced and set as a variable to check the shear reinforcement effect. Through quasi-static cyclic loading experiment, the seismic performance and shear behavior of the joint were examined for the failure mode, hysteresis performance, and energy-dissipation capacity of the specimens.

## 2 Research Significance

Previous studies have confirmed that it is possible to improve the shear force at the PC joint due to the high compressive strength and tensile strength of HPC and reinforcing fiber. When UHPFRC is used, it is expected that the performance can be satisfied while minimizing the crack width of the joint despite the reduction of the shear reinforcement at the joint. In order to utilize UHPFRC, it is necessary to confirm the effect of changing the binder combination for economical mixing and the performance change according to the reduction of shear reinforcement bars considering the shear reinforcement of UHPFRC. An experiment study was devised to assess joint reinforcement and usefulness of UHPFRC in PC beam–column joint.

## 3 Experiment

A half-scale exterior beam–column joint with seismic reinforcement details was designed and manufactured based on ACI 352R-02 to evaluate the performance of a PC beam–column joint connected using UHPFRC. Seven exterior beam–column connections were fabricated with four variables: (1) grouting performance; (2) beam end cross-sectional shape (grouting volume); (3) shear reinforcement at the joint core and beam end; and (4) corbel at the top of the lower column. To compare the effect of grouting performance, non-shrinkage mortar (which is

widely employed in conventional PC joint grouting) was used in addition to UHPFRC, and the cross-section from the end of the beam to a certain distance was changed to a U-shape to consider workability. Specimens with reduced shear reinforcement at the end of the beam and the joint core were fabricated and compared to confirm the shear reinforcement effect due to the UHPFRC, and a column corbel was applied to improve the constructability of the fieldwork and to separate the location of the plastic hinge from the joint. Table 1 presents the details of the specimens.

Figs. 1, 2 depict the cross-section of each specimen and the details of the corresponding arrangement, respectively respectively (Yuksel et al., 2015). The total length of the column was 1800 mm, and the length of the beam facing the column was 1350 mm. The column section was 250×250 mm, and the beam section was 200×300 mm. The 8-D19 main rebars were placed in the column, and shear rebars were placed with D10 at intervals of 60 mm near the junction and 120 mm in other sections. For the beam tension and compression rebars, 4-D13 were placed, and the shear rebars were D10, with an interval of 60 mm at the beam end and 120 mm at the center. In the PJ-CUS and PJ-CUS-C specimens with reduced shear rebars, the number of shear rebars in the joint core was reduced from five to three, and the number of shear reinforcement bars at the end of the beam was reduced from two to one (Yan et al., 2018). The longitudinal rebars of the beam were manufactured by exposing the 90° hook rebars in the same manner as the seismic details of the cast-in-place concrete, and the upper column and the lower column were connected with main reinforcement bars, and the joint core was empty, so the main reinforcement bars were exposed. After connecting the beams and installing shear reinforcement bars at the joint, the main reinforcement bars of beam were constrained, and the joint specimen was completed by grouting with mortar or UHPFRC.

For the PC member, a general 27 MPa ready mixed concrete was used, and for the non-shrinkage mortar, a

**Table 1** Summary of test specimens

Specimens	Grouting	Beam section	Reinforcement	Corbel
PJ-MR	Non-shrinkage mortar	Rectangle	Detail. 1	Not apply
PJ-CR	UHPFRC	Rectangle	Detail. 1	Not apply
PJ-MU	Non-shrinkage mortar	U-shaped	Detail. 1	Not apply
PJ-CU	UHPFRC	U-shaped	Detail. 1	Not apply
PJ-CUS	UHPFRC	U-shaped	Detail. 2	Not apply
PJ-CU-C	UHPFRC	U-shaped	Detail. 3	Apply
PJ-CUS-C	UHPFRC	U-shaped	Detail. 4	Apply

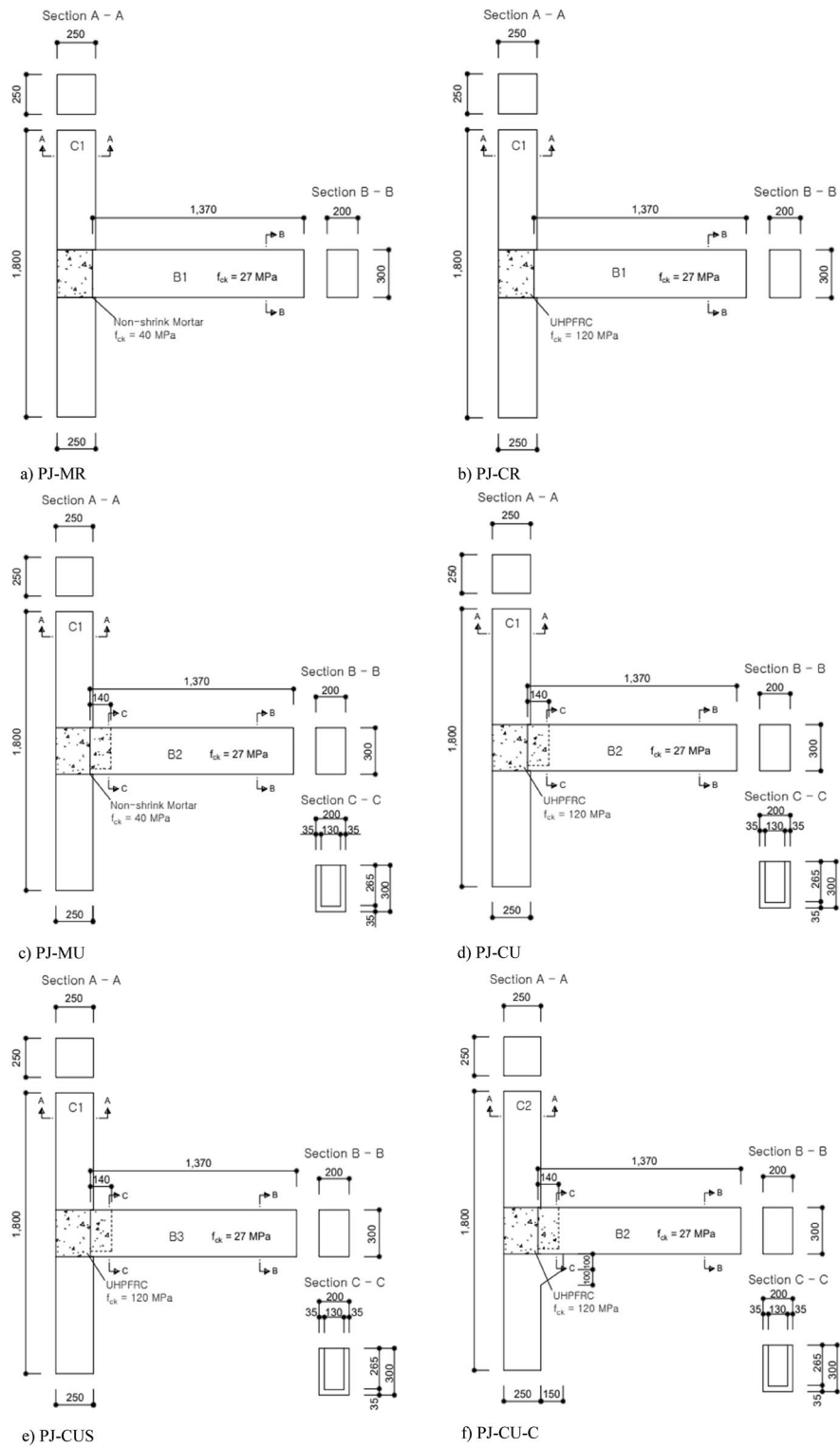


**Fig. 1** Section and rebar details of specimens (unit: mm)

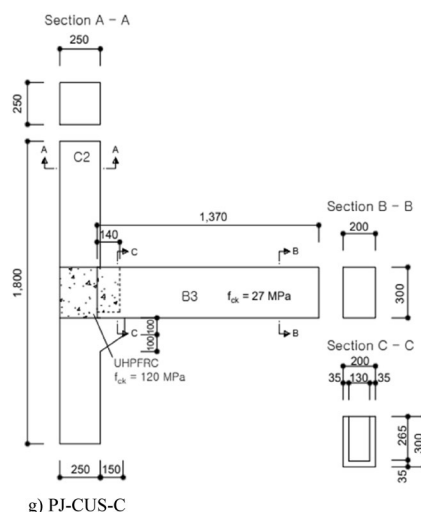


Fig. 1 continued

commercially available 40 MPa product was used. For the UHPFRC, a composition with a compressive strength of 120 MPa was employed, and needle-shaped high-strength steel fibers were mixed as reinforcing fibers. Table 2 shows the mixing ratio of UHPFRC used in the experiment. The binder combination was cement and silica fume, and the fine aggregate used was silica sand and river sand with particle size of 20 to 40 mesh. Silica flour were used as fillers with a silica content of over 99% and particle size of 12.4  $\mu\text{m}$ . The diameter of the mixed steel fibers was 0.2 mm, and lengths of 16 mm and 19 mm were mixed in a 2:1 ratio (Li et al., 2019). SD400 rebar was used as the reinforcement bar. Fig. 3 shows the compressive and bending strength test results of UHPFRC. The compressive strength was over 120 MPa and the bending strength was over 30 MPa. This mix was used for grouting PC joints. Table 3 outlines the properties of the mixtures used in these experiments.

Linear variable displacement transducer (LVDT) was installed to measure the specimens' deformation. Four LVDT were installed, two of which were installed on the beam surface to measure the displacement and rotation of the member, while another two were installed on the joint core to measure shear deformation. The setup for the cyclic loading experiments is presented in Figs. 4, 5. The end of the column was fixed, and a load was applied horizontally to the end of the beam. It is common to set the column end (corresponding to the central part of the actual structure) as pinned in light of the actual behavior. Thus, it is expected that there will be a difference from previous studies because the moment appears differently in the column part. Given this, an analysis was performed, focusing on the behavior of the beam and

joint core. The load was applied using an actuator with a capacity of 980 kN, and the cyclic load consisted of eight cycles with a drift ratio of 0.5% to 5%. Each cycle was set to three periods to apply the load in a displacement control method. Fig. 6 portrays the cyclic loading history.

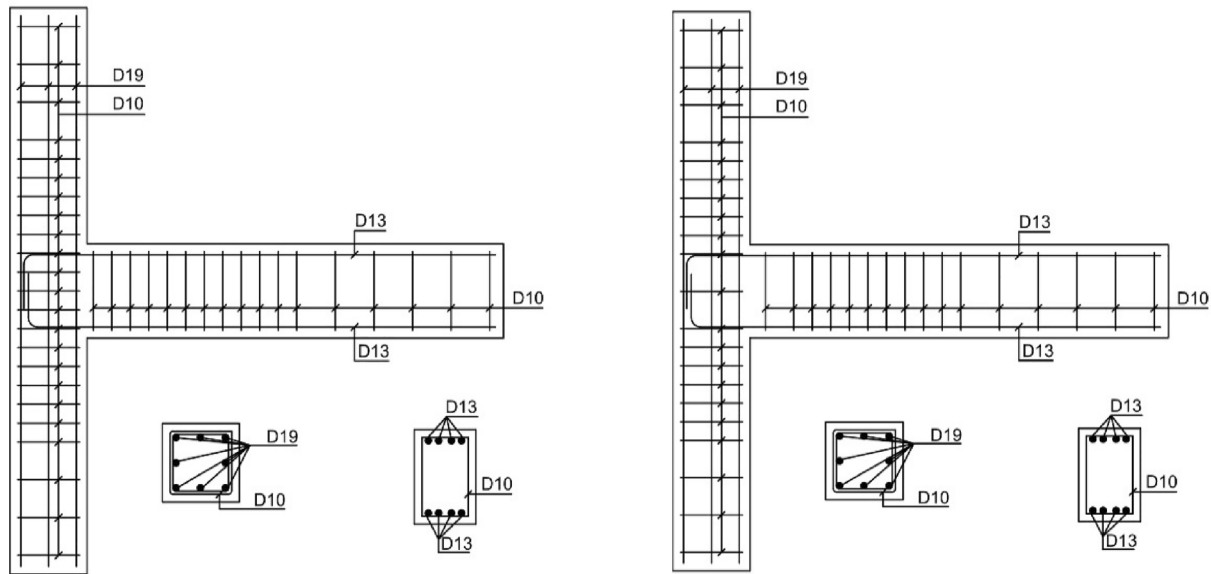
#### 4 Test Results

To analyze the performance of the PC joint, the test results of the beam–column joint were analyzed by dividing them into three categories: (1) crack and failure mode, (2) load–displacement curve, and (3) joint shear distortion.

##### 4.1 Crack and Failure Mode

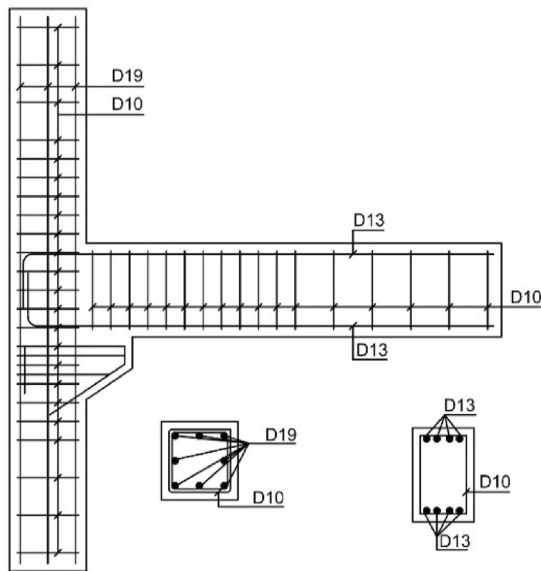
Fig. 7 shows the crack patterns of all the specimens. The black area indicates the location at which the concrete was delaminated as the crack width increased. Seismic details were applied; therefore, cracks occurred mainly in the beam area rather than inside the joints of all the specimens. By comparing PJ-MR and PJ-CR, it was confirmed that almost no cracks occurred in the joint core using UHPFRC. However, crack width widens in the end of the beam the area where the concrete was delaminated was increased. The shear reinforcement of the joint was made possible using UHPFRC.

In the PJ-MR specimen, a diagonal crack occurred at the beam end at a drift ratio of 3%, and a diagonal crack occurred in the joint core. The crack width of the core was very small compared to that of the beam, and the concrete peeling at the end of the beam was not significant. In the PJ-CR specimen, diagonal cracks began to appear at the end of the beam at a drift ratio of 1.5%. From a drift ratio of 3%, the crack width increased

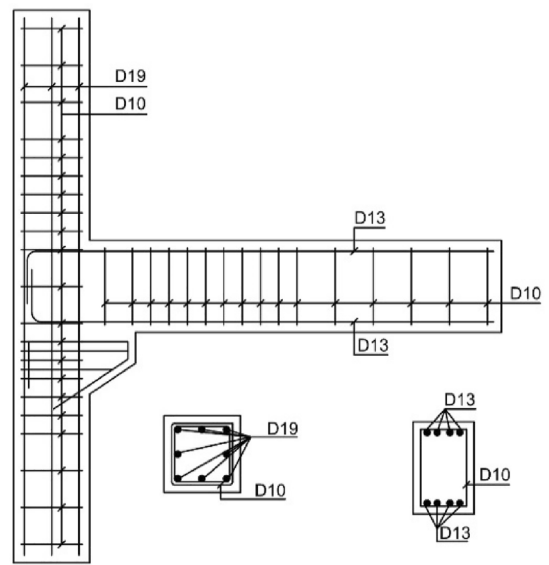


a) Detail-1

b) Detail-2



c) Detail-3



d) Detail-4

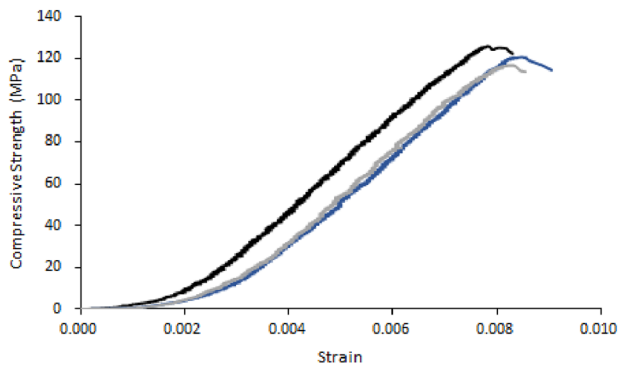
**Fig. 2** Reinforcement details

**Table 2** Unit weight of UHPFRC (unit: kg/m<sup>3</sup>)

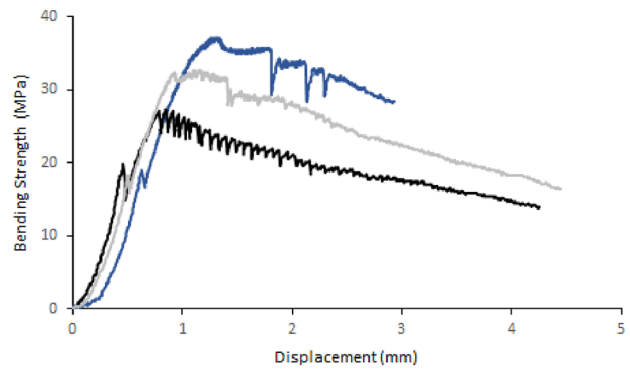
Water	Cement	Silica fume	Quartz sand	River sand	Silica flour	SP	Steel fiber
180	783	180	470	470	235	42	77.5

significantly, and peeling was noted. Notwithstanding, in the joint, cracks emerged only at the interface between the UHPFRC and the cast-in-place concrete, and no

cracks were seen in the joint core. The effect of shear at the end of the beam increased significantly due to a rise in the shear force at the joint. In the PJ-MU specimen,



a) Compressive strength



b) Bending strength

**Fig. 3** Strength curve of UHPFRC

**Table 3** Concrete strength

	Compressive strength (MPa)	Bending strength (MPa)
Ready mixed concrete	27	–
Non-shrinkage mortar	45	–
UHPFRC	121.0	32.3

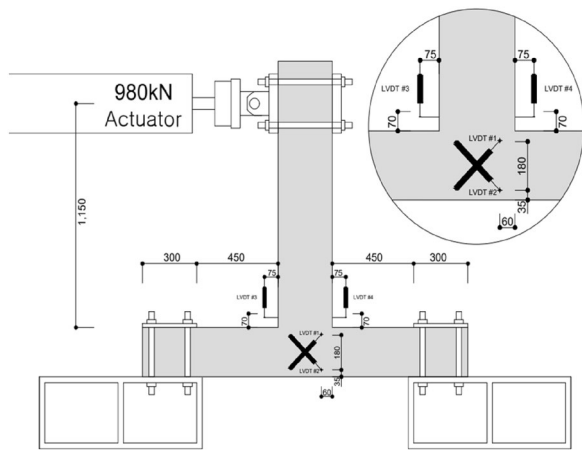


**Fig. 4** Schematic of test setup



**Fig. 5** Testing frame, boundary conditions and LVDT positions of PJ-CU specimen

diagonal cracks were observed at the end of the beam at a drift ratio of 1.5%; subsequently, the number of cracks did not rise significantly, the width of the diagonal cracks widened significantly, and the cast-in-place concrete part formed a U-shaped delamination phenomenon. In the joint core, several diagonal cracks with a compression zones occurred under the influence of shear (Gil-Martínet al., 2019). Similar to PJ-MU and PJ-CU had a diagonal crack at the end of the specimens, PJ-CU-C and

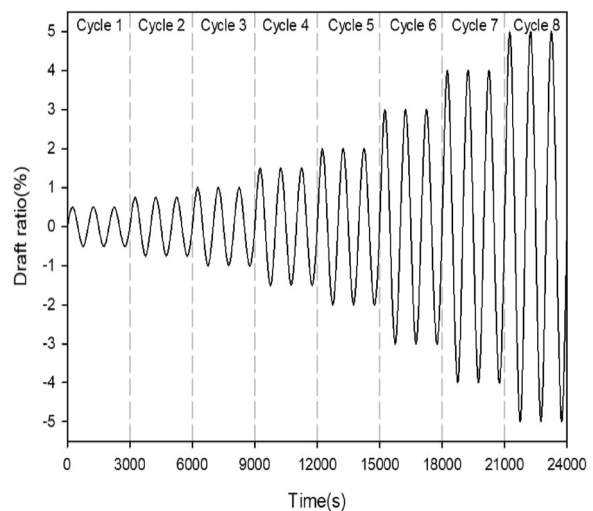


**Fig. 6** Cyclic loading history

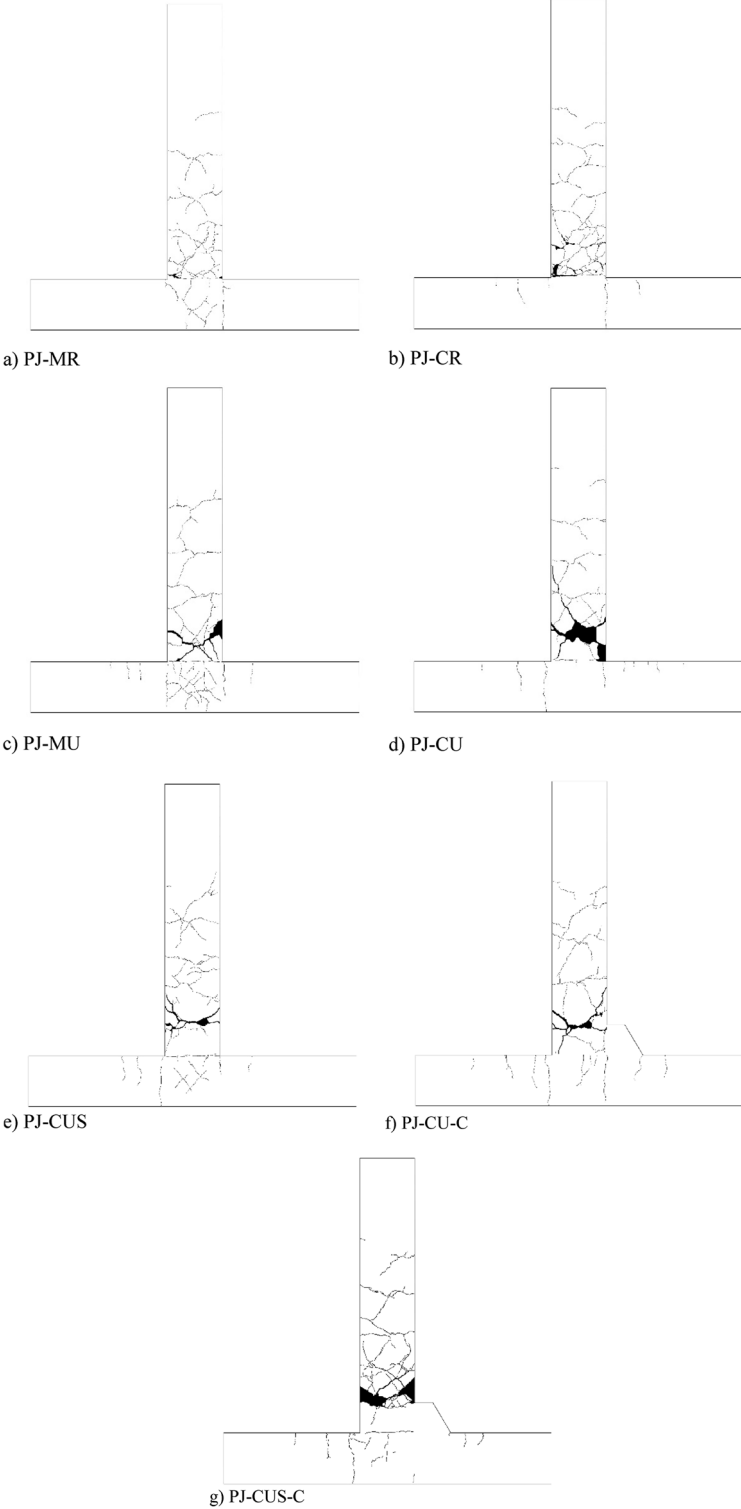


**Fig. 7** Crack formation and failure mode

PJ-CUS-C showed diagonal cracks in the inner section of the corbel; however, the crack width did not increase significantly. At the point where the corbels of the column and beam met, a horizontal crack appeared, and concrete delamination occurred as the crack width increased.

In the joint core, no large cracks were noted despite the decline in shear reinforcement, and the number of cracks and crack width increased in PJ-CUS-C compared to those in PJ-CU-C because of the decrease in shear reinforcement bars.

All specimens displayed the same failure mode as the failure occurring in the beam area, and the shear reinforcement effect of UHPFRC was confirmed by the inside of the joint and the crack pattern of the beam. When observing the crack pattern, the plastic hinge area moved to the UHPFRC casting surface. Given the shear reinforcement effect of the UHPFRC, the failure mode was the same, even when the shear reinforcement was reduced in the joint core. Moreover, the number and width of cracks did not appear significantly inside the joint, despite the decrease in shear reinforcement in the cracked area compared with the case where non-shrinkage mortar was used.

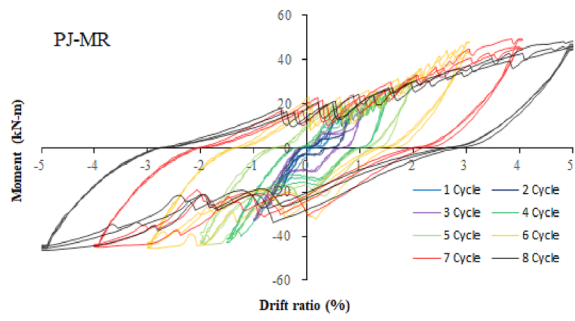
#### 4.2 Load–Displacement Relationship

Fig. 8 shows the results of the beam load versus displacement of the beam–column connection. Table 4 summarizes the design moments, peak moments, and corresponding drift ratios. The drift ratio was obtained by dividing the beam displacement by the distance from the load point at the end of the beam to the center of the column. Regarding the graph pattern, strength and stiffness degradation, as well as pinching were observed at the same drift ratio as that in the general hysteretic response. In the graph of the PJ-MR specimen, the maximum load was not accurately measured because the specimen and support moved during the experiment (Fig. 9).

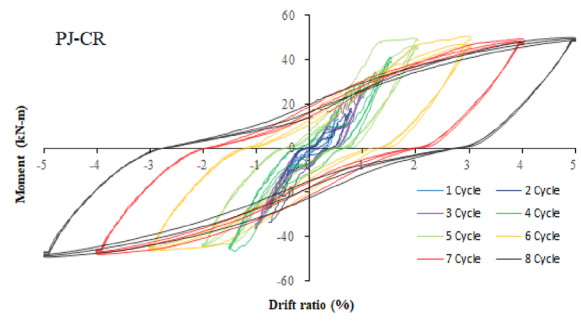
The maximum moment was recorded at a drift ratio of 3.85%, and strength degradation occurred at the same drift ratio. PJ-CR showed a slightly higher maximum moment than PJ-MR, but there was no significant difference. However,  $\delta_{peak}$  was 2.95%, which is lower than that of PJ-MR. Significant strength and stiffness degradations were seen within the maximum drift ratio of 3.00%, where the maximum moment was observed. Nevertheless, when the drift ratio increased, the maximum moment did not decline significantly, and the strength and stiffness degradation decreased. In PJ-MU, the strength degradation pattern was viewed more clearly than that in PJ-CR, and according to cycle repetition, the strength degradation was large at a drift ratio of 3.00%; this was the same as when the crack width started to increase significantly.

The maximum strength of the PJ-CU specimen increased compared with that of the PJ-MU specimen, but the crack width significantly increased at the interface between the cast-in situ concrete and the concrete peeled off, resulting in a significant strength degradation at a drift ratio of 5.00%. In the PJ-CUS specimen, the maximum moment was noted at a drift ratio of 3.00%, after which strength degradation was observed. However, strength degradation was seen compared to PJ-CU, which is considered to be due to the decline in the shear force concentrated on the beam due to the decrease in shear reinforcement bars in the connection. PJ-CU-C and PJ-CUS-C exhibited similar maximum strength. That said, PJ-CUS-C with reduced shear reinforcement exhibited slightly greater strength degradation.

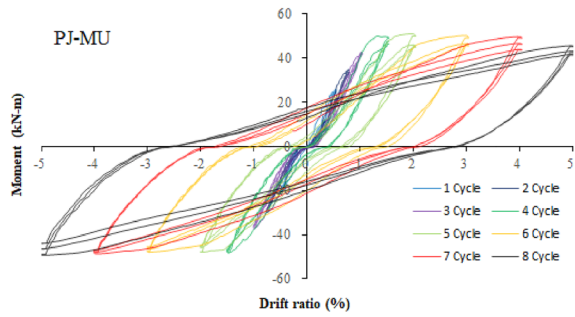
The specimens grouted with UHPFRC displayed a maximum load at a draft ratio higher than that in the case where the non-shrinkage mortar was applied, and similar results were obtained after the maximum load. Maximum strength was observed in the specimen with reduced shear reinforcement bars, which was considered to be caused by the shear reinforcement effect of the UHPFRC, and failure occurred while receiving a larger load at the beam (rather than at the joint). Owing to the effect of the corbel, the beam inside the corbel did not receive a large load; therefore, concrete peeling was reduced. As a result, a fairly small strength degradation was seen in the PJ-CU-C specimen compared to that in the PJ-CU specimen. When UHPFRC or non-shrinkage mortar was applied only to the inside of the joint, the maximum load was almost the same. However, the strength of specimens with a U-shaped beam area improved by 10–20% when UHPFRC was applied. The shear reinforcement of the joint core was determined by applying UHPFRC. Notwithstanding, the UHPFRC reinforcement at the end of the beam was not sufficient to change the failure mode. Reinforcing with UHPFRC in addition to the joint core is judged to have an effect only on increasing the cost of the member, rather than producing a significant change. In addition, in a study using high-strength concrete for the PC joint, the failure mode changed from brittle shear failure of the joint to beam end failure, and a strong joint design principle was achieved. That said, column end failure also occurred, confirming the need for column reinforcement to meet the strong column requirements. Therefore, in the case of a PC joint to which UHPFRC is applied, the joint reinforcement is sufficient, even if the reinforcement area is limited and applied within the joint core; this would be effective at improving the strength of the PC beam and column while maintaining the strong column principle. Table 4 summarizes the test results of moment and drift. Paulay et al. (1992) used a model to calculate the ductility of specimens. Specimens using



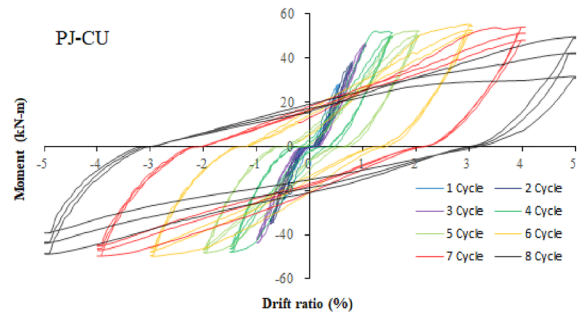
a) PJ-MR



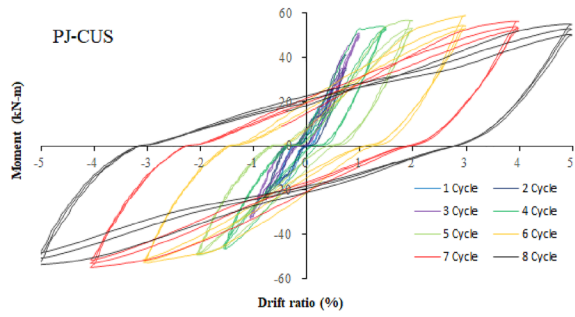
b) PJ-CR



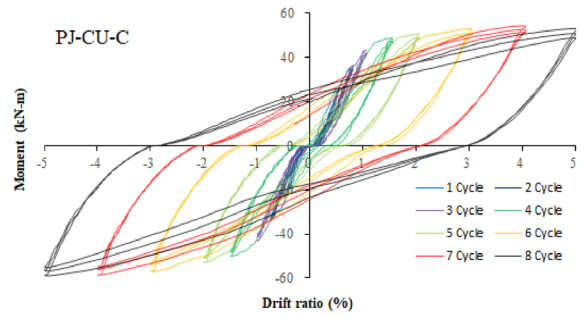
c) PJ-MU



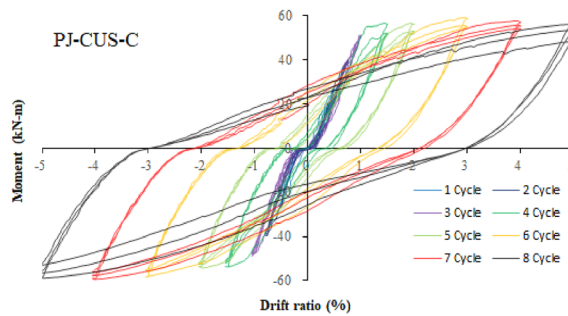
d) PJ-CU



e) PJ-CUS



f) PJ-CU-C

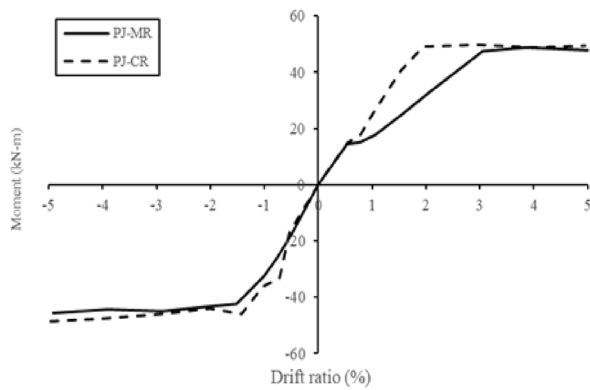


g) PJ-CUS-C

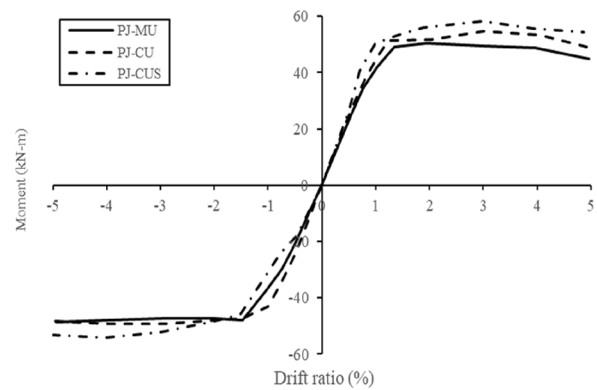
Fig. 8 Load-displacement curve

**Table 4** Beam moment and drift ratio of beam–column joint

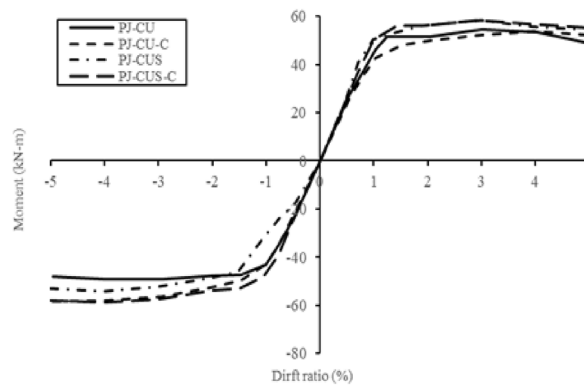
Specimen	$M_n$ (kN·m)	$M_{peak}$ (kN·m)	$\delta_{peak}$ (%)	$M_y$ (kN·m)	$\delta_y$ (%)	$\mu$
PJ-MR	55.0	48.84 (– 45.81)	3.85	36.63 (– 34.36)	2.62	1.07
PJ-CR		49.92 (– 48.70)	2.95	37.03 (– 36.52)	2.22	1.43
PJ-MU		50.32 (– 48.68)	3.01	37.74 (– 36.51)	1.27	1.60
PJ-CU		54.54 (– 49.23)	3.00	40.91 (– 36.92)	1.69	1.86
PJ-CUS		58.18 (– 54.23)	3.00	43.64 (– 40.67)	1.59	1.76
PJ-CU-C		53.61 (– 58.23)	3.99	40.21 (– 43.67)	1.65	1.22
PJ-CUS-C		58.40 (– 58.76)	2.93	43.80 (– 44.07)	1.57	1.60



a) Beam of rectangle cross-section



b) Beam of U-shaped cross-section



c) Column corbel

**Fig. 9** Backbone envelopes of lateral load–drift relations

UHPFRC exhibited higher ductility than non-shrinkage mortar, and specimens with grouting applied to the beam end with a U-shaped cross-section showed higher ductility than the case where grouting was applied only to the joint core. Compared to the case where grouting was applied only to the joint core, the test section demonstrated higher ductility. The corbel slightly reduced

the ductility of the joint, and lowering the shear reinforcement bar at the joint slightly decreased ductility. However, specimens with reduced shear reinforcement showed a slight increase in ductility in the presence of corbels.

The seismic performance of the tested PC joints was evaluated based on the acceptance criteria in ACI

**Table 5** Comparisons between test results and ACI 374.1–05 acceptance criteria (1)

Acceptance criteria	PJ-MR (+)	PJ-MR (-)	PJ-CR (+)	PJ-CR (-)	PJ-MU (+)	PJ-MU (-)	PJ-CU (+)	PJ-CU (-)
$\frac{M_{peak}}{M_n}$	0.89	0.83	0.91	0.89	0.91	0.89	0.99	0.90
During third cycle of 4% drift cycles								
$\frac{M_{3rd}}{M_{peak}}$	0.92	0.98	0.97	0.98	0.89	0.97	0.89	0.91
$\beta$	1.304		1.395		1.351		1.299	
$\frac{K_s}{K}$	0.17	0.24	0.43	0.39	0.29	0.22	0.17	0.13

$M_n$ : nominal beam moment strength (calculated based on measured material properties)

$M_{peak}$ : peak beam moment (measured)

$M_{3rd}$ : peak beam moment during 3rd cycle of 4.0% drift ratio (measured)

$\beta$ : relative energy dissipation ratio (ACI 374.1–05)

$K_s$  (+): secant stiffness for positive loading\* from a drift ratio of – 0.35% to a drift ratio of + 0.35% (ACI 374.1–05)

$K_s$  (-): secant stiffness for negative loading\*\* from a drift ratio of – 0.35% to a drift ratio of + 0.35% (ACI 374.1–05)

$K$  (+): initial stiffness for positive loading\* for first cycle (ACI 374.1–05)

$K$  (-): initial stiffness for negative loading\*\* for first cycle (ACI 374.1–05)

\* Positive loading, defined as loading from right to left (see Fig. 5)

\*\* Negative loading, defined as loading from left to right (see Fig. 5)

374.1–05. ACI 374.1–05 specifies the experimental results of the third complete

$$\gamma = \frac{(L1 - L2)\sqrt{l_1^2 + l_2^2}}{2 \times l_1 \times l_2} \tag{1}$$

cycle with a drift ratio not less than 3.5% should meet the following criteria for bi-directional response to satisfy the performance of the moment frame: (a) Peak force for a given loading direction shall have been not less than 0.75 of the maximum lateral resistance in the same loading direction; (b) the relative energy dissipation ratio shall have been not less than 0.125; and (c) the secant stiffness from a drift ratio of - 0.35% to a drift ratio of +0.35% shall have been not less than 0.05 times the initial stiffness during the first cycle for the same direction. In this analysis, the 4.0% drift ratio cycles were used in a conservative sense, in that 3.5% drift ratio cycles were not existed in the tests. Tables 5, 6 summarize the test results corresponding to the ACI 374.1.05 acceptance criteria. As shown in column 2 of Tables 5, 6,  $M_{peak}/M_n$  of all specimens was lower than 1.0, so the drift ratio will be larger than the limiting initial drift ratio defined as  $\Delta a/\phi C_d$ , which typically ranges between 0.3 and 0.5%. Considering that it is not  $M_n$  applied the characteristics of the PC joint and that typical statically determinate test systems much more flexible than real structures, it is judged that it will be difficult to accurately evaluate whether the standard is satisfied. However, by satisfying all acceptance criteria except for the limiting initial drift ratio, the performance of all specimens was deemed satisfactory. The test specimen that showed the greatest average strength degradation over three cycles at a deformation angle of

4% was PJ-CU at 10%, followed by PJ-MU at 7%. The remaining test specimens showed similar results of 5 to 6%, with PJ-CR showing the lowest average strength degradation at 2.5%. The specimen with U-shaped showed lower energy dissipation ratio ( $\beta$ ) and lower secant stiffness around zero drift ( $K_s/K$ ). It is believed that this is because the stress concentration of the beam due to the increase in the shear strength of the joint accelerated the deterioration of the bond between the U-shaped protruding normal concrete and UHPFRC. The higher energy dissipation ratio and secant stiffness of PJ-CUS, which reduces the shear reinforcement bars of the joint and beam compared to PJ-CU, is believed to be due to decrease in the stress concentration of the beam due to decrease of shear strength of the joint. Comparing PJ-CU and PJ-CU-C, an increase in energy dissipation ratio and secant stiffness was confirmed by applying corbels, but there was no significant difference in PJ-CUS and PJ-CUS-C even with the application of corbels. It was likely because, that the confining effect of shear reinforcement and grouting by shear reinforcement increased with the application of UHPFRC, reducing the effect of plastic hinge movement due to the corbel (Girgin et al., 2017).

### 4.3 Joint Shear Distortion

To measure the shear strain of the joint, LVDTs were installed in the joint core in two directions, and joint shear distortion was calculated using Eq. (1)(Chang and Han, 2021, Choi and Choi, 2014, Kim et al., 2016).

In the PJ-MR and PJ-MU test specimens using non-shrinkage mortar, shear cracks occurred in the diagonal direction at the joints. Fig. 10 outlines the load-joint shear distortion graph of each specimen. The test results

**Table 6** Comparisons between test results and ACI 374.1-05 acceptance criteria (2)

	Acceptance criteria	PJ-CUS (+)	PJ-CUS (-)	PJ-CU-C (+)	PJ-CU-C(-)	PJ-CUS-C (+)	PJ-CUS-C (-)	
During third cycle of 4% drift cycles	$\frac{M_{peak}}{M_n}$	≤ 1.25	1.06	0.99	0.97	1.06	1.06	1.07
	$\frac{M_{3rd}}{M_{peak}}$	≥ 0.75	0.94	0.94	0.95	0.94	0.94	0.95
	$\beta$	≥ 1.25	1.394		1.359		1.295	
	$\frac{K_s}{K}$	≥ 0.05	0.17	0.20	0.26	0.18	0.18	0.19

$M_n$ : nominal beam moment strength (calculated based on measured material properties)

$M_{peak}$ : peak beam moment (measured)

$M_{3rd}$ : peak beam moment during 3rd cycle of 4.0% drift ratio (measured)

$\beta$ : relative energy dissipation ratio (ACI 374.1–05)

$K_s$  (+): secant stiffness for positive loading\* from a drift ratio of - 0.35% to a drift ratio of +0.35% (ACI 374.1–05)

$K_s$  (-): secant stiffness for negative loading\*\* from a drift ratio of - 0.35% to a drift ratio of +0.35% (ACI 374.1–05)

$K$  (+): initial stiffness for positive loading\* for first cycle (ACI 374.1–05)

$K$  (-): initial stiffness for negative loading\*\* for first cycle (ACI 374.1–05)

\* Positive loading, defined as loading from right to left (see Fig. 5)

\*\* Negative loading, defined as loading from left to right (see Fig. 5)

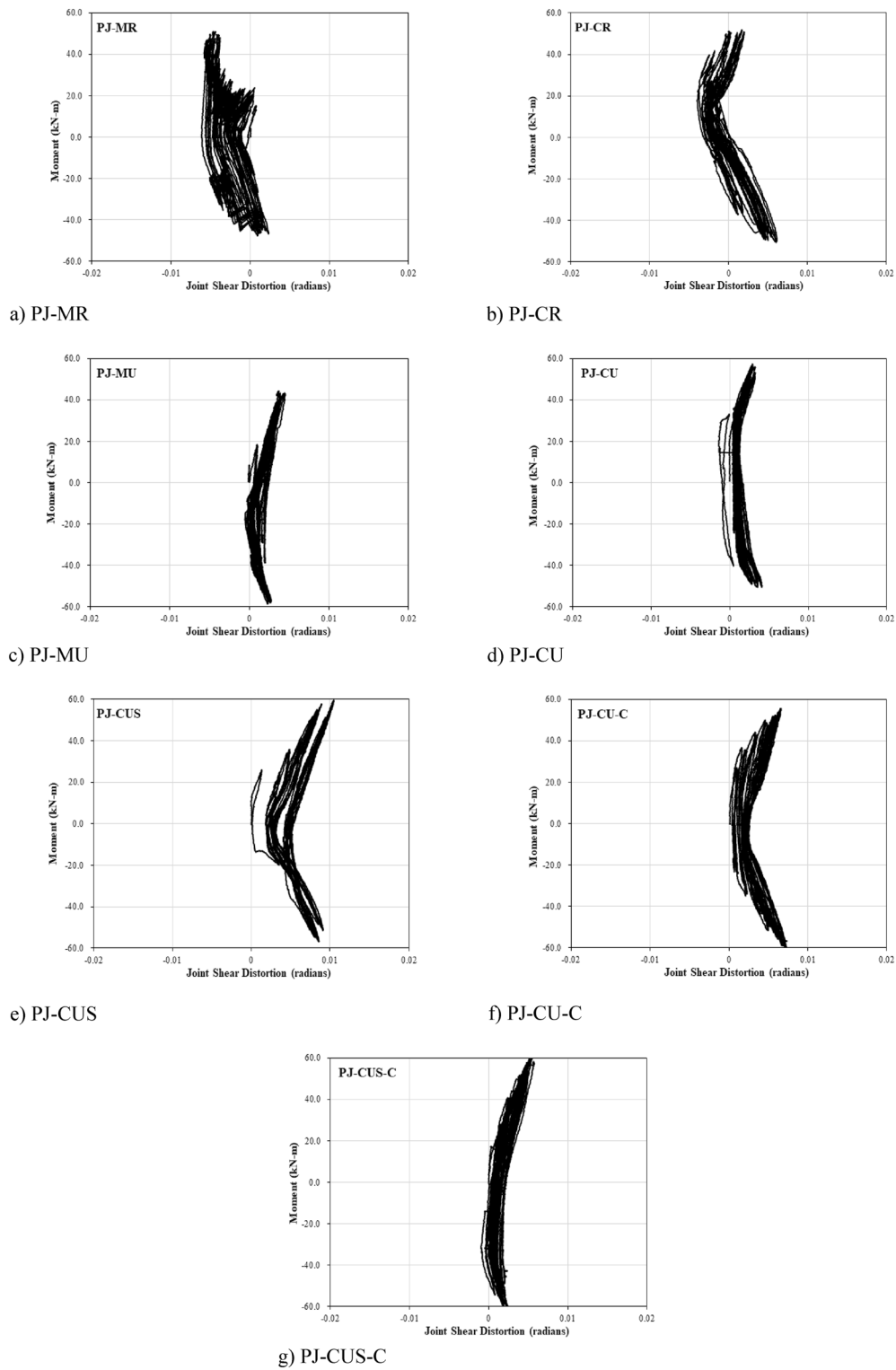


**Fig. 10** Load vs. joint shear distortion curve

indicate that most of the specimens were restrained within 0.01 rad of shear deformation, and only the PJ-CUS specimens with reduced shear reinforcement exceeded 0.01 rad at the maximum load. Comparing PJ-MR, PJ-CR, PJ-MU, and PJ-CU, the shear strain decreased when UHPFRC was used, which was attributed to the incorporation of steel fibers.

## 5 Conclusion

In this study, an experiment was performed to evaluate the seismic performance of PC beam–column joints using UHPFRC and non-shrinkage mortar as grouting. The shear reinforcement effect of the joint (based on the application of UHPFRC) and the applicability of UHPFRC to PC joints were analyzed in terms of strength and joint shear distortion. The following conclusions were drawn:

1. The test specimen to which the non-shrinkage mortar was applied had diagonal cracks in the joint core, whereas the specimen to which UHPFRC was applied had no cracks in the joint core. The reinforcement effect was deemed to be as good as that of shear reinforcement bars.
2. Given the on-site construction of the PC joint, the test specimen with a U-shaped cross-section of the beam end boosted fracture strength by increasing the grouting area. The area where concrete peeling was noted due to the occurrence of a plastic hinge appeared at the interface between the grouting and the cross-section of the PC member. Based on the fluidity of UHPFRC, there is no great merit in improving on-site workability compared to the labor required to manufacture U-shaped beam members.
3. An increase in joint moment was confirmed by applying UHPFRC, and degradation was significantly observed in PJ-CU. In the case of PJ-CU, it seems to be influenced by the fact that large separation occurred due to lack of adhesion at the interface between normal concrete and UHPFRC at the cross-section of the beam. The U-shaped beam considering workability is not judged to be of great merit, and it is judged that applying corbels and separating PC beams of rectangular cross-section from the column surface promotes structural safety by moving the plastic hinges and is advantageous in terms of manufacturing and constructability.
4. All specimens of PC beam–column joint conformed to all performance acceptance criteria in ACI 374.1–05, except for the limiting initial drift ratio. The average strength degradation during the third cycle at a 4.0% drift ratio was only about 10% at the maximum, in PJ-CU, and it was confirmed that the U-shaped beam considering field construction can accelerate the deterioration of the bond. The PC joint met the standards for energy dissipation ratio ( $\beta$ ) and secant stiffness around zero drift ( $K_s/K$ ), but the measured moment was about 30% lower than the design moment.
5. Shear reinforcement and crack reduction in the joint core were confirmed by applying UHPFRC. However, the stress at the end of the beam was found to be higher than that of the test specimen subjected to non-shrinkage mortar. As a result, as the end shear crack width increased, significant concrete delamination occurred at the same drift ratio, and significant strength degradation was observed. Since the test specimen with reduced shear reinforcement in the joint core showed a decrease in strength degradation, UHPFRC as a PC joint grouting would be effective in mitigating the congestion of the reinforcement bars in the joint core with sufficient shear reinforcement.

### Acknowledgements

This research was supported by "Leaders in INdustry-university Cooperation 3.0 (LINC3.0)" Project funded by the Ministry of Education and National Research Foundation of Korea. The staff assistance at the HPSEM Lab of Kumoh National Institute of Technology is highly appreciated for the fabrication and testing of the specimens.

### Author contributions

All authors contributed to the research reported in the paper. The authors confirm their contribution to the paper as follows: conceptualization, SK, JS and WK; formal analysis, SK and WK; funding acquisition, WK; investigation, SK, JS and WK; methodology, SK and WK; supervision, WK; project administration, WK; writing—original draft, SK and JS; writing—review and editing, SK, JS and WK. All authors read and approved the final manuscript.

### Funding

This research was supported by "Leaders in INdustry-university Cooperation 3.0 (LINC3.0)" Project funded by the Ministry of Education and National Research Foundation of Korea.

### Availability of data and materials

Manuscript does not include any individual person's data.

### Declarations

#### Competing interests

The authors declare that they have no known competing interests or personal relationships that could have appeared to influence the work reported in this paper.

Received: 29 June 2023 Accepted: 18 September 2023

Published online: 09 February 2024

### References

- Chang, H., Choi, I., Kim, J., & Hong, S. Y. (2021). Experimental investigation on seismic performance of two types of member-panel zone unified joints for precast concrete moment-resisting. *Journal of Building Engineering*. <https://doi.org/10.1016/j.jobe.2021.103202>

- Chang, Y. S., & Han, S. W. (2021). Seismic behavior of corner beam-column joints reinforced with HPFRCC based on cyclic tests. *Journal of the Korea Concrete Institute*. <https://doi.org/10.4334/JKCI.2021.33.5.441>
- Choi, H. K., & Choi, C. S. (2014). Classification schemes of precast beam-column connections according to contribution of deformation components. *Journal of the Korea Concrete Institute*, 26(4), 545–553. <https://doi.org/10.4334/JKCI.2014.26.4.545>
- Choi, H. K., Choi, Y. C., & Choi, C. S. (2013). Development and testing of precast concrete beam-to-column connections. *Engineering Structures*, 56, 1820–1835. <https://doi.org/10.1016/j.engstruct.2013.07.021>
- Deng, M., Ma, F., Song, S., Lü, H., & Sun, H. (2020). Seismic performance of interior precast concrete beam-column connections with highly ductile fiber-reinforced concrete in the critical cast-in-place regions. *Engineering Structures*. <https://doi.org/10.1016/j.engstruct.2020.110360>
- Dong, Y. H., Jaillon, L., Chu, P., & Poon, C. S. (2015). Comparing carbon emissions of precast and cast-in-situ construction methods—a case study of high-rise private building. *Construction and Building Materials*, 99, 39–53. <https://doi.org/10.1016/j.conbuildmat.2015.08.145>
- Ghayeb, H. J., Razak, H. A., & Sulong, N. H. R. (2020). Seismic performance of innovative hybrid precast reinforced concrete beam-to-column connections. *Engineering Structures*. <https://doi.org/10.1016/j.engstruct.2019.109886>
- Gil-Martín, L. M., Rodríguez-Suesca, A. E., Fernández-Ruiz, M. A., & Hernández-Montes, E. (2019). Cyclic behavior of RC beam-column joints with epoxy resin and ground tire rubber as partial cement replacement. *Construction and Building Materials*, 211, 659–674. <https://doi.org/10.1016/j.conbuildmat.2019.03.216>
- Girgin, S. C., Misir, I. S., & Kahraman, S. (2017). Experimental cyclic behavior of precast hybrid beam-column connections with welded components. *International Journal of Concrete Structures and Materials*, 11(2), 229–245. <https://doi.org/10.1007/s40069-017-0190-y>
- Husam, S., Viktoria, W., Clemens, M., Stefan, B., Ekkehard, F., & Alexander, W. (2019). Environmental assessment of ultra-high-performance concrete using carbon. *Material, and Water Footprint, MAterials*, 12(6), 851. <https://doi.org/10.3390/ma12060851>
- IPCC. (2007). Climate change 2007 – Synthesis report. Contribution of Working Groups I, II and III to the Fourth Assessment Report of the Intergovernmental Panel on Climate Change.
- Kim, S. H., Kwon, B. U., & Kang, T. H. K. (2016). Seismic performance assessment of roof-level joints with steel fiber-reinforced high-strength concrete. *Journal of the Korea Concrete Institute*, 28(2), 235–244. <https://doi.org/10.4334/JKCI.2016.28.2.235>
- Li, L., Cai, Z., Yu, K., Zhang, Y. X., & Ding, Y. (2019). Performance-based design of all-grade strain hardening cementitious composites with compressive strengths from 40 MPa to 120 MPa. *Cement and Concrete Composites*. <https://doi.org/10.1016/j.cemconcomp.2019.01.001>
- Lin, Y., Chen, Z., Guan, D., & Guo, Z. (2021). Experimental study on interior precast concrete beam-column connections with UHPC core shells. *Structures*, 32, 1103–1114. <https://doi.org/10.1016/j.istruc.2021.03.087>
- Maya, L. F., Zanuy, C., Albajar, L., Lopez, C., & Portabella, J. (2013). Experimental assessment of connections for precast concrete frames using ultra high performance fibre reinforced concrete. *Construction and Building Materials*, 48, 173–186. <https://doi.org/10.1016/j.conbuildmat.2013.07.002>
- Na, Y., Han, B., & Son, S. (2021). Analysis of CO<sub>2</sub> emission reduction effect of on-site production precast concrete member according to factory production environment. *Advances in Civil Engineering*. <https://doi.org/10.1155/2021/4569651>
- Parastesh, H., Hajirasouliha, I., & Ramezani, R. (2014). A new ductile moment-resisting connection for precast concrete frames in seismic regions: an experimental investigation. *Engineering Structures*, 70, 144–157. <https://doi.org/10.1016/j.engstruct.2014.04.001>
- Paulay, T., & Priestly, M. J. N. (1992). Seismic design of reinforced concrete and masonry buildings. *A Wiley Interscience Publication*. <https://doi.org/10.1002/9780470172841>
- Wahjudi, D. I., Suprobo, P., & Sugihardjo Tavio, S. (2014). Behavior of precast concrete beam-to-column connection with U- and L-bent bar anchorages placed outside the column panel—experimental study. *Procedia Engineering*, 95, 112–121. <https://doi.org/10.1016/j.proeng.2014.12.170>
- Yan, X., Wang, S., Huang, C., Qi, A., & Hong, C. (2018). Experimental study of a new precast prestressed concrete joint. *Applied Sciences*. <https://doi.org/10.3390/app8101871>

- Yuksel, E., Karadogan, H. F., Bal, I. E., Ilki, A., Bal, A., & Inci, P. (2015). Seismic behavior of two exterior beam-column connections made of normal-strength concrete developed for precast construction. *Engineering Structures*. <https://doi.org/10.1016/j.engstruct.2015.04.044>

## Publisher's Note

Springer Nature remains neutral with regard to jurisdictional claims in published maps and institutional affiliations.

**Seungki Kim** Seungki Kim is a Ph.D. candidate in the Department of Architectural Engineering at the Kumoh National Institute of Technology.

**Jinwon Shin** Jinwon Shin is an Assistant Professor in the Department of Architectural Engineering at the Catholic Kwandong University.

**Woosuk Kim** Woosuk Kim is an Associate Professor in the School of Architecture at the Kumoh National Institute of Technology.

Submit your manuscript to a SpringerOpen® journal and benefit from:

- Convenient online submission
- Rigorous peer review
- Open access: articles freely available online
- High visibility within the field
- Retaining the copyright to your article

Submit your next manuscript at ► [springeropen.com](https://www.springeropen.com)